Organic Geochemistry 121 (2018) 68–79

Contents lists available at ScienceDirect

Organic Geochemistry

journal homepage: www.elsevier.com/locate/orggeochem

Determination and geochemical implication of multiple series of long-chain oxygen-bearing compounds trapped in kerogen in the Lucaogou Formation, Santanghu Basin, NW China

Bin Cheng [a], Jianbing Xu [a,b], Yungan Liang [a,b], Qian Deng [a,b], Yankuan Tian [a], Zewen Liao [a,*]

[a] State Key Laboratory of Organic Geochemistry, Guangzhou Institute of Geochemistry, Chinese Academy of Sciences, Guangzhou 510640, China
[b] University of Chinese Academy of Sciences, Beijing 100049, China

ARTICLE INFO

Article history:
Received 25 March 2018
Accepted 9 April 2018
Available online 11 April 2018

Keywords:
n-Aldehyde
n-Alkan-2-one
Stable carbon isotope
Kerogen
Santanghu Basin

ABSTRACT

Studies of occluded oxygen-bearing compounds inside kerogen are scarce, although such studies are important in understanding early-stage transformation of organic matter. A relatively low-maturity kerogen from the late Permian mudstone of the Lucaogou Formation of the Santanghu Basin, northwestern China, was successively extracted with *n*-hexane, acetone and dichloromethane to release the adsorbed components, and the extracted kerogen was treated with a mild oxidation reagent H_2O_2 to release the occluded components. Gas chromatography–mass spectrometry analysis of the adsorbed and occluded components revealed a suite of oxygen-bearing compounds, including *n*-alkan-2-ones, *n*-aldehydes and fatty acid methyl esters. The *n*-alkan-2-ones were mainly detected in the adsorbed fraction and *n*-aldehydes in the occluded component. Comparison of the long-chain oxygen-bearing compound distributions and their individual stable carbon isotope characteristics both suggest that the oxygen-bearing compounds released by H_2O_2 treatment were occluded in the kerogen. The shorter-chain (C_{15} to C_{19}) occluded *n*-aldehydes reflected similar isotopic distribution trends to the adsorbed *n*-alkan-2-ones, and the $\delta^{13}C$ values of the mid-length (C_{21} to C_{25}) occluded *n*-aldehydes were much closer to the adsorbed *n*-alkanes. Bacterially mediated methylation and decarbonylation of the *n*-aldehydes during kerogen formation may be important source(s) of *n*-alkan-2-ones and *n*-alkanes, respectively. The mid-chain ketones mainly originated from hydrothermal alteration of *n*-alkanes after kerogen formation. Uplift of the Lucaogou Formation in the Yuejingou section allowed surface-enhanced aerobic reactions.

© 2018 Elsevier Ltd. All rights reserved.

1. Introduction

During formation and evolution of "proto-kerogen", some smaller molecules including biomarkers are adsorbed to, occluded in or bonded to the macromolecular structure (Snowdon et al., 2016; Wu and Geng, 2016; Cheng et al., 2017). Components that are easily extracted from the periphery of the "proto-kerogen" by conventional organic solvents are referred to as the adsorbed fraction, while free components in the macromolecular core structure that are difficult to extract by conventional organic solvents are considered as the occluded fraction (Cheng et al., 2016, 2017). The molecules occluded inside (Behar et al., 1984; Ekweozor, 1984, 1986; Liao and Geng, 2002; Liao et al., 2006a; Khaddor et al., 2008; Zhao et al., 2012) or bound in (Cassani and Eglinton, 1986; Love et al., 1998; Russell et al., 2004) the geomacromolecular structure are believed to retain organic geochemical information of earlier maturity stages (e.g., before or during kerogen formation) preserved by the protection of the macromolecular structure. Most studies of occluded or bound components have investigated the saturated hydrocarbons (e.g., Behar et al., 1984; Ekweozor, 1984, 1986; Cassani and Eglinton, 1986; Love et al., 1998; Liao and Geng, 2002; Russell et al., 2004; Liao et al., 2006a,b; Khaddor et al., 2008; Lockhart et al., 2008; Zhao et al., 2010, 2012; Cheng et al., 2014a,b, 2015, 2016, 2017; Snowdon et al., 2016; Wu and Geng, 2016), although studies of oxygen-bearing compounds from kerogen pyrolysis have also appeared in the literature (e.g., Gillaizeau et al., 1996; Riboulleau et al., 2000; Grice et al., 2003; Zhang et al., 2016). Few studies of occluded oxygen-bearing compounds in geomacromolecules have been reported.

In the early maturity stages, many oxygen-bearing compounds such as fatty acids, fatty alcohols, aliphatic ketones, fatty acid esters and others, are present in sedimentary organic matter (Tissot and Welte, 1984). These are mainly derived from their

* Corresponding author.
E-mail address: liaozw@gig.ac.cn (Z. Liao).

https://doi.org/10.1016/j.orggeochem.2018.04.005
0146-6380/© 2018 Elsevier Ltd. All rights reserved.

natural precursors and are closely related to biological markers (Peters et al., 2005). After kerogen formation, these compounds are dispersed or adsorbed around the kerogen macromolecule (e.g., Song et al., 2004; Wang et al., 2012, 2016), bound to the kerogen (e.g., Gillaizeau et al., 1996; Riboulleau et al., 2000; Zhang et al., 2016), and may also be occluded inside the kerogen structure. Studies of the occluded oxygen-bearing compounds in the kerogen are helpful in our understanding of early-stage deposition and evolution features of organic matter.

Wang et al. (2012, 2016) found several series of linear oxygen-bearing compounds in the soluble fractions of the Lucaogou Formation source rocks from the Tiaohu Sag (Yuejinggou profile, well Tiao-5) and Malang Sag (wells Ma-6 and Ma-7) in the Santanghu Basin, northwestern China. These included fatty acids, fatty acid methyl esters and *n*-alkan-2-ones, all of which are likely derived from early-stage microbial degradation (Wang et al., 2012), but their specific origin and evolution remained unclear.

In the present study, the kerogen of the Lucaogou Formation mudstone was selected for study by releasing the adsorbed and occluded components. The origin and evolution of the long-chain oxygen-bearing compounds from the soluble fraction of the mudstone are discussed in terms of their geochemical characteristics in contrast to the ones trapped in the kerogen. The role of the oxygen-bearing compounds on hydrocarbon generation in the Lucaogou Formation source rocks was also studied.

2. Geological setting

2.1. Structural pattern of Santanghu Basin

The Santanghu Basin is located at the northeastern margin of Xinjiang Uygur Autonomous Region, China, bordering the Republic of Mongolia to the north and adjacent to the Tuha Basin in the south, and covering a narrow zone from northwest to southeast. Since the late Paleozoic, the region has experienced four tectonic evolution stages: basement formation to oceanic crust extinction (Carboniferous); evolution of an intracontinental foreland basin (early Permian to late Permian); basin uplift and depression (Upper Triassic to Lower Cretaceous); and finally, basin transformation since the Upper Cretaceous (Zhao et al., 2003; Liu et al., 2010; Wu et al., 2011). Strong tectonic movement during the late Yanshan–Himalayan period has not only led to the first-order structural alternations in the Santanghu Basin but has also resulted in the structural alterations of rise–sag in the central depression region (Li et al., 2004).

The first-order structural units comprise the Northeast Fold and Thrust Belt, the Central Depression Belt and the South Fold and Thrust Belt from northeast to southwest. The second-order structural units from northwest to southeast (Fig. 1) comprise five rises and four sags – the Hanshuiquan Sag, Shitoumei Rise, Tiaohu Sag, Chahaquan Rise, Malang Sag, Fangfangliang Rise, Naomaohu Sag, Weibei Rise and Suluke Sag.

2.2. Depositional environment of the Lucaogou Formation

The Santanghu Basin evolution began as an intracontinental foreland basin after the Carboniferous (Zhao et al., 2003; Liu et al., 2010; Wu et al., 2011) and experienced a depositional facies transition from residual marine trough to terrestrial lacustrine with continuing fall in sea level (Xu et al., 2013). In the middle Permian it evolved into a sediment-starved intracontinental rift basin, accompanied by mantle-originated movement of hydrothermal fluids (Liu et al., 2012; Li et al., 2013; Hackley et al., 2016). Weak volcanism during the deposition of the Lucaogou Formation resulted in the development of mudstones, lime mudstones, dolomitic mudstones and other fine-grained sediments forming the source rocks of the Lucaogou Formation (Gao et al., 2010; Ma et al., 2012, 2016).

The variety of marine and non-marine fossils found in the Lucaogou Formation supports the finding of a transition of sedimentary facies from residual marine trough to terrestrial lacustrine (Li and Liang, 2001; Yin et al., 2002). The significant decrease in sulfur content and increase in total organic content (TOC) upwards from the base of the Lucaogou Formation are further evidence of

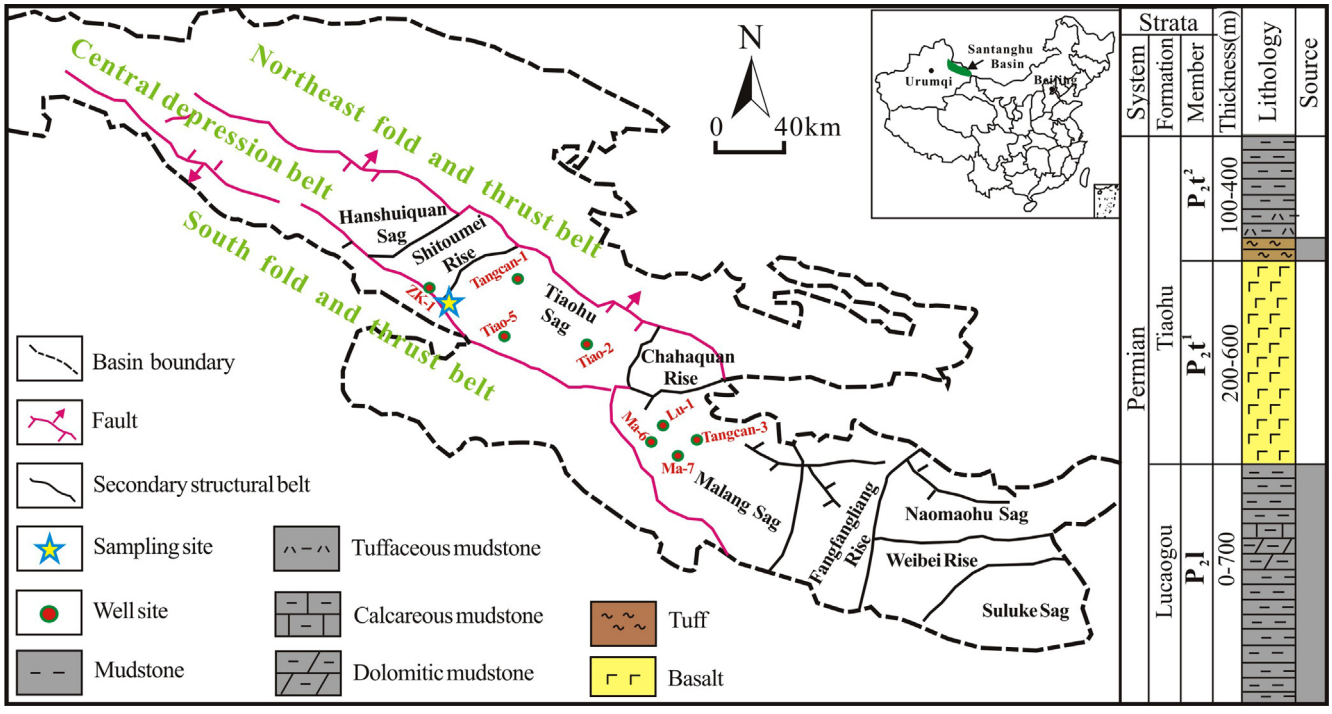

Fig. 1. Santanghu Basin and the sample locality used in this study (from Ma et al. (2016), with minor modification).

falling sea level and increasing freshwater inflow into the basin (Tao et al., 2017). Studies of *n*-alkanes and biomarkers such as terpanes and steranes have shown that the parent biomass of the Lucaogou Formation source rocks was derived from both aquatic organisms and terrestrial higher plants deposited in a brackish to highly saline lacustrine environment (Liu et al., 2015, 2017; Cheng et al., 2016; Hackley et al., 2016). Basing on the redox- and salinity-sensitive proxies (e.g., V/Cr, V/(V + Ni), Sr/Ba, Rb/K, B/Ga ratios), together with the wide distribution of pyrite and carbonate minerals in these dark, thinly laminated organic-rich rocks, Tao et al. (2017) and Zhang et al. (2018) suggested that dysoxic–anoxic, brackish–saline, arid–sub-humid, and alkaline conditions prevail during deposition of the Lucaogou Formation.

3. Experimental

3.1. Sample

Late Permian Lucaogou Formation (P_2l) calcareous mudstone was selected from the Yuejinggou section of the Santanghu Basin, northwestern China (Fig. 1). The grey-black sample was buried by loess from 0.5 m to 1 m deep and was slightly weathered. After cleaning in water and drying, the sample was ground to particles of 0.18 mm diameter. The powdered mudstone was treated with HCl and HF to isolate the kerogen (precise details of this treatment process can be found in Vandenbroucke and Largeau, 2007).

3.2. Organic solvent extraction and mild oxidation treatment

The isolated kerogen was Soxhlet extracted with *n*-hexane, acetone and dichloromethane consecutively for 120 h (Fig. 2) to obtain the adsorbed components. Benzene (40 mL) was used as solvent (dispersant) for oxidation treatment while H_2O_2/CH_3COOH (about 10 mL/10 mL) served as the oxidation system for the extracted residual kerogen (≈5 g). The blends were then allowed to react for 48 h under magnetic stirring at room temperature, and the product was filtered through a Büchner funnel by adding dichloromethane. The obtained liquid phase was then transferred to a 250 mL polytetrafluoroethylene (PTFE) separating funnel, and ultrapure water was added to separate the organic and inorganic phases. The detailed procedure and method is shown in Fig. 2 and described in Cheng et al. (2015, 2016).

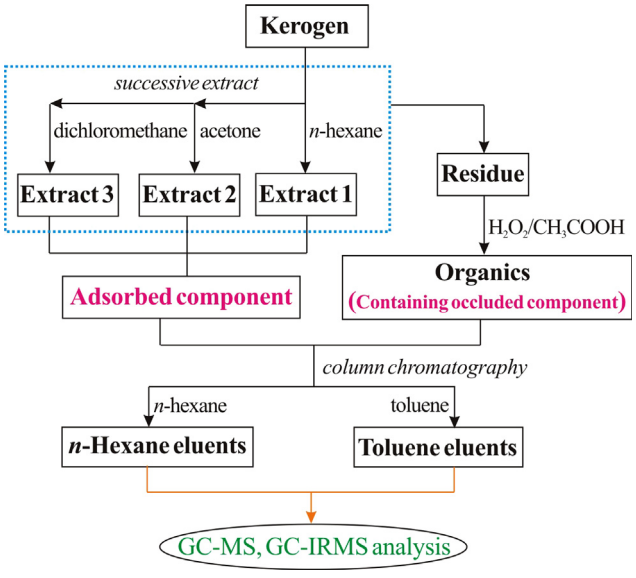

Fig. 2. Schematic flowchart of the sample treatment and instrumental analyses.

The solvent extracts (adsorbed components) and the organic phase of the oxidation products (containing occluded components) were further separated by column chromatography using a 9 cm column containing silica gel:aluminum oxide (3:1) and eluted with 15 mL of *n*-hexane and 12 mL of toluene to yield a saturated fraction and aromatic fraction, respectively. These fractions were separately analysed using gas chromatography–mass spectrometry (GC–MS). The *n*-alkanes and *n*-alk-2-ones from the *n*-hexane extract and the *n*-alk-1-enes and *n*-aldehydes from the oxidative degradation products were analysed using gas chromatography–isotope ratio mass spectrometry (GC–IRMS).

3.3. Instrumental analysis

3.3.1. Geochemical data analysis

Analyses performed on the calcareous mudstone included rock pyrolysis utilizing a Rock-Eval 6.0 standard pyrolysis analyzer, mineral analysis using an Olympus Innov-X BTX X-ray diffractometer (XRD) and trace element analysis using a Perkin-Elmer Elan 6000 inductively coupled plasma-mass spectrometer (ICP-MS). The element analysis for the kerogen was carried out using a Vario EL III element analyzer. A 3Y-Leica DMR XP microphotometer was used to measure the optical vitrinite reflectance of the sample, with 125 × oil microscope objective and immersion oil refractive index N = 1.515.

3.3.2. GC–MS analysis

The *n*-hexane and toluene fractions were analysed using a DSQ II and Thermo Fisher Trace GC Ultra combined system. The GC conditions were: HP-1 ms chromatographic column (60 m × 0.32 mm × 0.25 μm film thickness); helium as the carrier gas with a constant 1.2 mL/min flow mode. MS conditions used were: electron ionization mode; ion source electron energy 70 eV; ion source temperature 260 °C; and a mass scan range of 50–650 Da. The oven temperature ramp-up procedures were as follows: For the *n*-hexane fraction: 80 °C initial temperature held for 4 min, then raised to 295 °C at a rate of 4 °C/min and held isothermally for 20 min; For the toluene fraction: 80 °C initial temperature held for 4 min, then raised to 295 °C at a rate of 3 °C/min and held isothermally for 30 min.

3.3.3. GC–IRMS analysis

Stable carbon isotope analysis of low molecular weight compounds was done on an Isoprime (VG) mass spectrometer combined with an Agilent 6890 GC. Except for using a DB-5 column (30 m × 0.32 mm × 0.25 μm film thickness), the GC conditions and temperature ramp-up procedure were as for the GC–MS analysis described in Section 3.3.2. Carbon isotope values are reported in per mil (‰) relative to the defined Vienna PDB standard. Replicate analyses showed the reproducibility was generally within ±0.5‰. Results are reported as the average of two or three runs.

4. Results

4.1. Geochemical data

The calcareous mudstone sample used in this work consisted mainly of albite, quartz, chlorite, dolomite and apatite, and small amounts of calcite and pyrite (Table 1), with albite as the main mineral comprising up to 51.0%. For the trace element distribution in the mudstone, Ti was dominant with up to 2866 ppm, which exceeded the total of all other trace elements. Trace elements (100–505 ppm) included Mn, Sr, Ba and Cr; other trace elements were <100 ppm. The ratios of Sr/Ba, Th/U, δU (2U/(U + Th/3)), V/(V + Ni) were 1.24, 1.08, 1.47 and 0.57, respectively (Table 2). The

Table 1
Mineral content of the mudstone (wt%).

Rock	Pyrite	Dolomite	Calcite	Albite	Quartz	Apatite	Chlorite
Value	3.1	8.9	5.3	51.0	13.0	8.6	10.1

Table 2
Trace element distribution of the mudstone.

Rock	Trace element content (ppm)										Sr/Ba	Th/U	2U/(U + Th/3)	V/(V + Ni)
	Ti	Mn	Sr	Ba	Cr	V	Ni	Th	U	∑others				
Value	2866	505	260	210	132	59.8	45.6	5.1	4.7	426	1.24	1.08	1.47	0.57

vitrinite reflectance (%Ro) of the kerogen was 0.52 (Table 3); T_{max} was 436 °C; and Production Index (PI) was 0.01 (Table 4), indicating a low thermal maturity. The free hydrocarbon content (S1) of the rock was 0.57 mg/g, while that of the cracked hydrocarbons (S2) was 53.1 mg/g. The high S2 value, together with the TOC value of 10.67% determined by pyrolysis, indicates that the mudstone contains a high organic matter content.

The isolated kerogen contained 72.75% C, 8.22% H, 12.87% O, 2.41% N and 2.01% S (Table 3), accounting for 98.26% of the total kerogen. The ratios of H/C, O/C and S/C (0.11, 0.18, 0.03) are consistent with a low-maturity kerogen.

After consecutively extracting with *n*-hexane, acetone and dichloromethane, the isolated kerogen extract yields were 0.96%, 1.31% and 0.04%, respectively (Table 5). The extracted kerogen was treated with H_2O_2/CH_3COOH and we obtained a dichloromethane extract of the oxidative degradation product up to 5.0% based on the isolated kerogen, obviously higher than the total organic solvent extractable yield of 2.41%.

4.2. Components from total ion chromatogram (TIC) in n-hexane fraction

The chromatograms of organic solvent extracts (adsorbed fraction) contained an unresolved complex mixture (UCM). Elemental sulfur species included S_6, S_7 and predominantly S_8 molecules (Cheng et al., 2016) (Fig. 3a). The C_{14}–C_{28} *n*-alkanes showed a predominance of *n*-C_{23}, with 25-norhopane and C_{29}–C_{30} hopanes also detected. A slight odd carbon preference was observed in the longer-chain *n*-alkane distribution (>C_{22} *n*-alkanes). Similar chromatograms were obtained for the acetone and dichloromethane extracts (Fig. 3b and c).

A series of even-carbon-numbered *n*-alk-(1)-enes and *n*-alkanes were detected from the occluded fraction of the kerogen, with *n*-alk-(1)-enes as the main suite of compounds (Fig. 3d). The even-carbon-numbered *n*-alk-1-enes were mostly from C_{16} to C_{32}, with a predominance of C_{22} and C_{24}. The *n*-alkanes ranged from C_{16} to C_{30}, indicating a similar distribution to that of the adsorbed fraction, but with a slight even-numbered carbon preference. The ratio of *n*-alk-1-ene/*n*-alkane (-ene/-ane for short) with the same carbon number was >1. Large amounts of sulfur, including S_6, S_7 and S_8 molecules, were also detected in the occluded fraction (Fig. 3d).

Table 5
Relative contents and group composition from the solvent extracts and the oxidative degradation products of kerogen.

Type	Extracts (%)	S (%)	A (%)	R (%)	A/S
$E_{n\text{-hexane}}$	0.96	8.24	5.78	85.98	0.70
$E_{acetone}$	1.31	0.10	0.19	99.71	2.00
$E_{dichloromethane}$	0.04	1.16	5.81	93.02	5.00
$E_{oxidation}$	5.00	0.57	1.27	98.16	2.25

Note: Extracts = solvent extracted components based on the initial isolated kerogen; S = saturated fraction; A = aromatic fraction; R = fraction other than saturated and aromatic fraction. $E_{n\text{-hexane}}$ = *n*-hexane extract from kerogen; $E_{acetone}$ = acetone extract from kerogen; $E_{dichloromethane}$ = dichloromethane extract from kerogen; $E_{oxidation}$ = dichloromethane extract of the oxidative degradation products.

4.3. Distribution of long-chain oxygen-bearing compounds

The aromatic fractions from the extracts and oxidative degradation product obtained from the toluene eluent were rich in oxygen-bearing compounds but poor in aromatic hydrocarbons, which may be related to the low thermal maturity of the kerogen. The oxygen-bearing compounds mainly contained 2,4-di-tert-butylphenol, ketones, fatty acid methyl esters, *n*-aldehydes and others. Table 5 shows that the oxygen-bearing compounds were rich both in the *n*-hexane extract and the oxidative degradation products. Because the oxygen-bearing compounds were determined generally as different groups, in the following paragraphs a descriptive terminology is used for the different types of compounds, which is not precise from the principle of IUPAC nomenclature but more easily followed by the reader.

Table 3
Element distribution of the kerogen and its vitrinite reflectance.

Kerogen	Element content (%)					H/C	O/C	S/C	%Ro
	C	H	O	N	S				
Value	72.75	8.22	12.87	2.41	2.01	0.11	0.18	0.03	0.52

Table 4
Rock-Eval data of the mudstone.

Rock-Eval	S1 (mg/g)	S2 (mg/g)	S3 (mg/g)	PI	HI (mg/g)	OI (mg/g)	Tmax (°C)	TOC (%)
Value	0.57	53.1	4.84	0.01	497	45	436	10.67

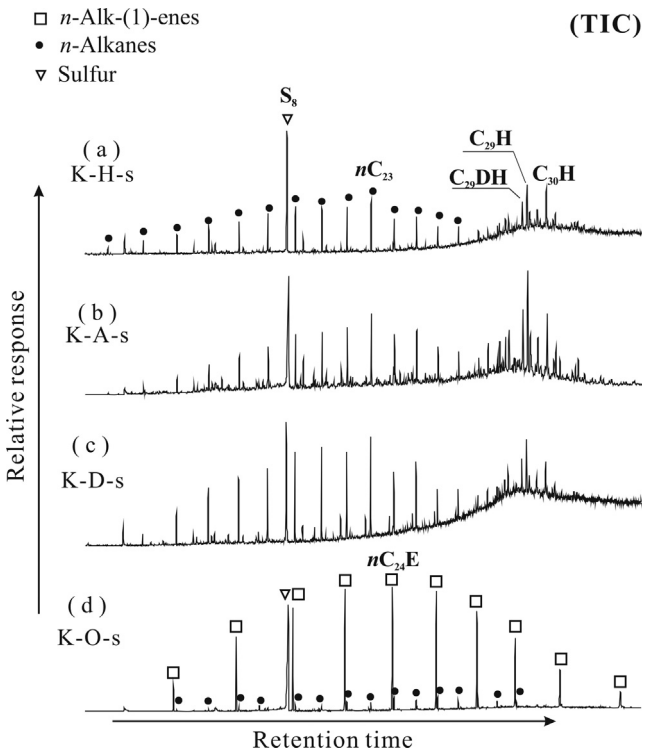

Fig. 3. Chromatograms of *n*-hexane eluents from the solvent extracts and oxidative degradation products of kerogen: (a) *n*-hexane extract; (b) acetone extract; (c) dichloromethane extract; and (d) oxidative degradation product. The compound assignments are listed in Table 6.

4.3.1. Ketones

Several series of straight-chain ketones were detected in the three solvent extracts, including *n*-alkan-2-ones, *n*-alkan-3-ones, *n*-alkan-4-ones, *n*-alkan-5-ones and *n*-alkan-9-ones, as well as isomeric 6,10,14-trimethylpentadecan-2-one ($iC_{18}K$) (Fig. 4). The alkan-2-ones, showing the typical base peak at *m/z* 58 (George and Jardine, 1994; Gobé et al., 2000; Guignard et al., 2005; Wang et al., 2012; Zhang et al., 2016), were the main components in the *n*-hexane fraction total ion chromatogram (TIC), but much less in the other two fractions and could only be observed from their *m/z* 58 mass chromatograms (Fig. 4a–c). These ketones, with the exception of *n*-alkan-3-ones, were also detected on the *m/z* 58 mass chromatogram of the oxidative degradation products (Fig. 4d).

As the isolated kerogen was successively extracted by *n*-hexane, acetone and dichloromethane, most ketones were included into the *n*-hexane fraction. Therefore, the ketones distribution characteristics in the *n*-hexane fraction can roughly represent the adsorbed components. The *n*-alkan-2-ones, from both the adsorbed and occluded fractions, displayed a unimodal distribution from C_{12} to C_{29} with a predominance of C_{20} ($nC_{20}K$) (Fig. 4a and d; Table 7). The *n*-alkan-(3–9)-ones in the adsorbed fraction showed a similar distribution to the *n*-alkan-2-ones (Fig. 4a), but with lesser abundance.

In Fig. 5, ratios of *n*-alkan-(4–9)-ones/*n*-alkan-2-ones showed almost the same distribution patterns via increasing carbon numbers for the adsorbed and occluded fractions, with higher values for the adsorbed fraction (also Table 8). As *n*-alkan-3-ones were not determined in the occluded fraction, they were not included in the above ratios. The ratios of *n*-alkan-(4–9)-ones/*n*-alkan-2-ones in the Yuejinggou section, as showed in Fig. 5, were very low in comparison to well Tiao-5 in the Tiaohu Sag or wells Ma-6 and Ma-7 in the Malang Sag of the Santanghu Basin (Wang et al., 2012).

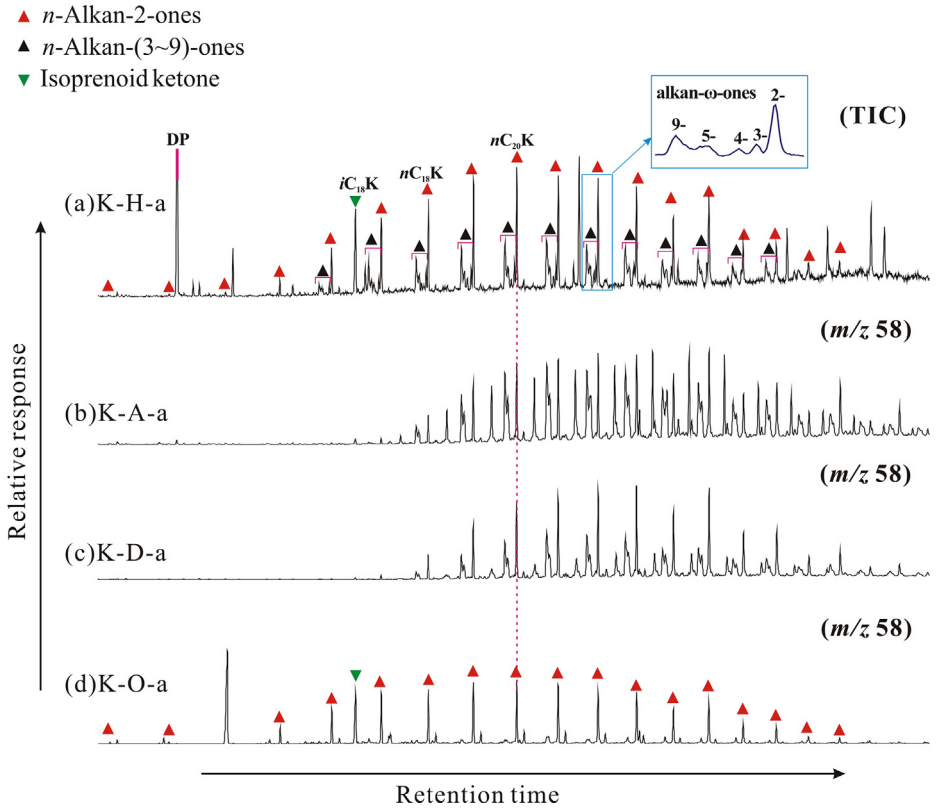

Fig. 4. Distributions of the alkan-2-ones in toluene eluents from the solvent extracts and oxidative degradation products of kerogen: (a) *n*-hexane extract; (b) acetone extract; (c) dichloromethane extract; and (d) oxidative degradation product. The compound assignments are listed in Table 6.

Table 6
Compound assignments for the peaks in Figs. 3, 4, 6 and 7.

Peak	Compound
nC_{23}	C_{23} *n*-alkane
S_8	Element sulfur
C_{29}DH	C_{29} 17α,21β(H)-25-norhopane
C_{29}H	C_{29} 17α,21β(H)-30-norhopane
C_{30}H	C_{30} 17α,21β(H)-hopane
nC_{24}E	C_{24} *n*-alk-1-ene
DP	2,4-di-tert-butylphenol
iC_{18}K	6,10,14-trimethylpentadecan-2-one
nC_{20}K	C_{20} *n*-alkan-2-one
C_{18}ME, C_{21}ME, C_{24}ME	C_{18}, C_{21} and C_{24} fatty acid methyl esters
nC_{11}A, nC_{16}A, nC_{20}A	C_{11}, C_{16} and C_{20} *n*-aldehydes

4.3.2. Fatty acid methyl esters

The concentration of fatty acid methyl esters was low both in the solvent extracts and oxidative degradation products and was only observed using a *m/z* 74 mass fragmentogram (Fig. 6). The spectra showed the typical base peak at *m/z* 74 for fatty acid methyl esters (Gobé et al., 2000; Guignard et al., 2005; Wang et al., 2012). The fatty acid methyl esters displayed a unimodal distribution ranging from C_{16} to C_{34} with a predominance of C_{21} (C_{21}ME) (Fig. 6), which was more evident in the dichloromethane extract than in the other fractions.

4.3.3. n-Aldehydes

The *n*-aldehydes were the main components in the TIC chromatogram of the oxidative degradation products, but in the solvent extracts they were only observable from the *m/z* 82 mass fragmentogram (Fig. 7). To confirm the identification of *n*-aldehydes, 97% pure C_{11} *n*-aldehyde (from Sigma-Aldrich) was selected as the standard compound. The toluene fraction from the oxidative degradation products and the C_{11} *n*-aldehyde standard were analysed by GC–MS using identical instrument conditions. The results showed the same peak times and ion fragment distribution for the C_{11} *n*-aldehyde standard and the C_{11} *n*-aldehyde from the oxidative degradation product. Moreover, addition of a specified amount of the C_{11} *n*-aldehyde standard to the toluene eluent of oxidative degradation product enhanced the indicated C_{11} *n*-aldehyde peak confirming the identification.

4.4. Stable carbon isotope of individual compounds

The *n*-alkanes and *n*-alkan-2-ones from the *n*-hexane fraction and the *n*-alk-1-enes and *n*-aldehydes from the oxidative degradation product were selected for compound specific isotope analysis and these results are shown in Fig. 8.

The $\delta^{13}C$ values of the even-numbered C_{18}–C_{36} *n*-alk-1-enes were −29.6‰ to −28.9‰, becoming slightly enriched in ^{13}C with increasing carbon numbers. The $\delta^{13}C$ values of C_{13}–C_{25} *n*-aldehydes were −37.6‰ to −30.4‰, with C_{15} and C_{18} molecules distinctly enriched whereas C_{22} to C_{28} were depleted in $\delta^{13}C$ (Fig. 8). The $\delta^{13}C$ values of the C_{16}–C_{28} *n*-alkanes were −36.9‰ to −33.1‰. With carbon number increase, the stable carbon isotopes of the *n*-alkanes displayed three distribution features as follows:

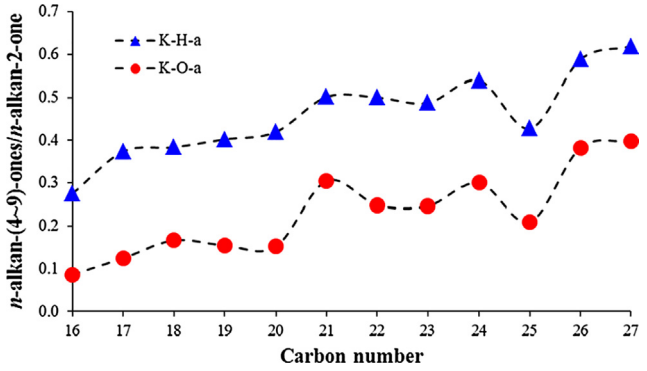

Fig. 5. Variations of *n*-alkan-(4–9)-one/*n*-alkan-2-one ratios with the increasing carbon number. Note: K-H-a and K-O-a represented those from toluene eluents of the adsorbed fraction and occluded fraction, respectively.

(1) for <C_{20} *n*-alkanes, slightly enriched in ^{13}C; (2) C_{20} to C_{25} *n*-alkanes, sharply depleted in ^{13}C via increasing carbon numbers; (3) >C_{25} *n*-alkanes, slightly enriched in ^{13}C again with increasing carbon number. This isotope distribution pattern is similar to the results of the Lucaogou mudstone samples in the Santanghu Basin reported by Liu et al. (2017).

The $\delta^{13}C$ values of C_{13}–C_{24} *n*-alkan-2-ones were −36.7‰ to −32.9‰, among which C_{14}-, C_{18}- and C_{21}–alkan-2-ones were distinctly depleted in ^{13}C compared to their neighboring compounds (Fig. 8). The $\delta^{13}C$ value of the isomeric 6,10,14-trimethylpentadecan-2-one (not indicated in Fig. 8, but see Fig. 4a) was −32.7‰, distinctly enriched in ^{13}C compared to all other *n*-alkan-2-ones.

For the *n*-alk-1-enes, *n*-aldehydes, *n*-alkanes and *n*-alkan-2-ones with the same carbon number, the order of $\delta^{13}C$ values was basically *n*-alk-1-enes > *n*-aldehydes > *n*-alkanes > *n*-alkan-2-ones, among which the *n*-alk-1-enes had remarkably enriched stable carbon isotope values (Fig. 8). In particular, the C_{15} and C_{18} *n*-aldehydes were enriched in ^{13}C compared to their neighbors, which was accompanied by the corresponding C_{16} and C_{19} *n*-alkan-2-ones also enriched in ^{13}C compared to their counterparts. However, >C_{20} *n*-aldehydes showed a closer isotope distribution relationship with the *n*-alkanes but diverged from the *n*-alkan-2-ones (Fig. 8).

The *n*-alk-1-enes had obviously enriched stable carbon isotopes than the other three series of compounds, perhaps implying a formation process different from the others. Cheng et al. (2014a) suggested that the *n*-alk-1-enes had been formed through a concerted or semi-concerted reaction of esters under a low thermal stress occurred in sedimentary organics. Possible formation pathways of the other three series of compounds detected in this work will be discussed in the following sections.

5. Discussion

5.1. Redox environments, organic evolution of the Lucaogou Formation

The series of *n*-alkanes detected in the *n*-hexane fraction, together with the UCM compounds in the TIC (Fig. 3a), implies a

Table 7
Carbon range and dominant compounds in the long-chain compound series.

Type	*n*-alkanes	*n*-alkan-2-ones	*n*-aldehydes	FAME
$E_{n\text{-hexane}}$	C_{14}–C_{28}/C_{23}	C_{12}–C_{29}/C_{20}	C_{13}–C_{28}/C_{20}	/
$E_{acetone}$	C_{14}–C_{27}/C_{23}	C_{17}–C_{28}/C_{20}	C_{13}–C_{28}/C_{20}	C_{16}–C_{34}/C_{21}
$E_{dichloromethane}$	C_{14}–C_{27}/C_{23}	C_{17}–C_{28}/C_{20}	/	C_{16}–C_{34}/C_{21}
$E_{oxidation}$	C_{16}–C_{34}/C_{22}–C_{24}	C_{12}–C_{29}/C_{20}	C_{10}–C_{30}/C_{20}	C_{16}–C_{34}/C_{21}

Note: $E_{n\text{-hexane}}$ = *n*-hexane extract; $E_{acetone}$ = acetone extract; $E_{dichloromethane}$ = dichloromethane extract; $E_{oxidation}$ = oxidative degradation products; FAME = fatty acid methyl esters. Taking $E_{n\text{-hexane}}$ as an example, C_{14}–C_{28}/C_{23} represented that the carbon range of *n*-alkanes was C_{14}–C_{28} with the C_{23} *n*-alkane as the predominant compound in the *n*-alkane series.

Table 8
Ketone ratios of *n*-alkan-(4–9)-ones/*n*-alkan-2-one from the adsorbed (K-H-a) and occluded (K-O-a) fractions.

Compound	C_{16}	C_{17}	C_{18}	C_{19}	C_{20}	C_{21}	C_{22}	C_{23}	C_{24}	C_{25}	C_{26}	C_{27}
K-H-a	0.28	0.37	0.38	0.40	0.42	0.50	0.50	0.49	0.54	0.43	0.59	0.62
K-O-a	0.09	0.13	0.17	0.16	0.15	0.31	0.25	0.25	0.30	0.21	0.38	0.40

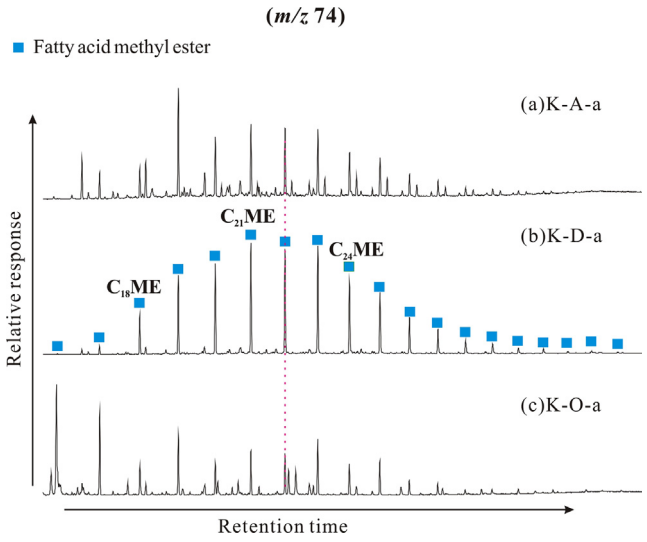

Fig. 6. Distributions of fatty acid methyl esters in the toluene eluents from the solvent extracts and the oxidative degradation products of kerogen: (a) acetone extract; (b) dichloromethane extract; and (c) oxidative degradation product. The compound assignments are listed in Table 6.

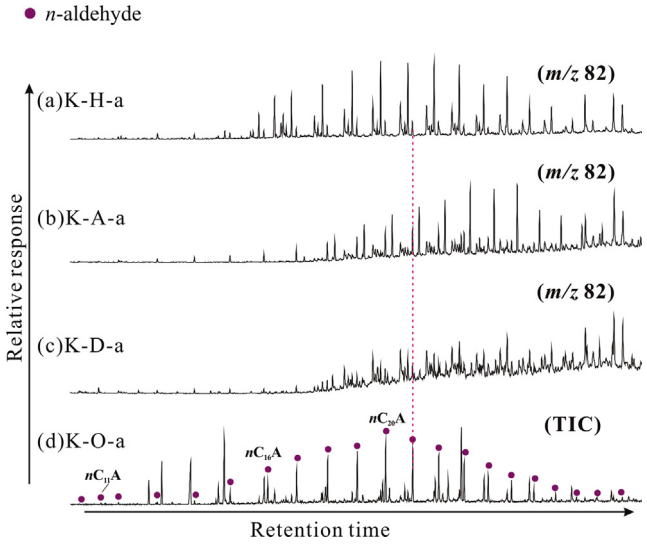

Fig. 7. Distributions of *n*-aldehydes in toluene eluents from the solvent extracts and the oxidative degradation products of the kerogen: (a) *n*-hexane extract; (b) acetone extract; (c) dichloromethane extract; and (d) oxidative degradation product. The compound assignments are listed in Table 6.

possible biodegradation process having occurred in the sedimentary organics. For example, the detection of 25-norhopanes has been considered as an indication for oil biodegradation (Jiang et al., 1990; Blanc and Connan, 1992), and they have been determined in the Permian source rocks of the Santanghu Basin (Bao, 1997; Du et al., 2004; Cheng et al., 2016), which have also been determined in this work (Fig. 3a and Table 6). Du et al. (2004) suggested that the 25-norhopanes detected in the Lucaogou Formation mudstone might have come from the original hopanoids, because this suite of source rocks has been exposed to microbial degradation either during deposition or in their early diagenetic stages.

Some redox-sensitive trace elements such as Th, U, Cr, Co, V and Ni are important indicators for the redox condition of ancient sedimentary water bodies. The trace element studies of the Lucaogou Formation rocks from wells YY1 (Zhang et al., 2017) and Zk-1 (Tao et al., 2017) in the Shitoumei Rise, and well Lu-1 (Zhang et al., 2018) in the Malang Sag suggested a dysoxic-anoxic depositional environment for the Lucaogou Formation source rocks. Tao et al. (2017) inferred a change from reducing conditions to oxidizing conditions upwards from the base of the Lucaogou Formation, based on redox-sensitive trace element studies.

Usually, ratios of Th/U < 2 (Wignall and Twitchett, 1996), δU(2 U/(U + Th/3)) > 1 (Steiner et al., 2001) and V/(V + Ni) > 0.6 (Jones and Manning, 1994) indicate an anoxic sedimentary environment, while the opposite cases suggest an oxic environment. The Th/U, 2U/(U + Th/3) and V/(V + Ni) ratios from the Lucaogou Formation mudstone in this work were 1.08, 1.47 and 0.57, respectively (Table 2), indicating an anoxic condition for the sedimentary mudstone. Elemental sulfur, as the product of incomplete oxidation in the inorganic sulfur cycle, can be either oxidized to form SO_4^{2-} or reduced to H_2S (Lin et al., 2015). Detection of abundant elemental sulfur in the Lucaogou Formation samples (including the mudstone and the isolated kerogen) in this work indicates that the sedimentary environment was not completely anoxic. The presence of series of *n*-aldehydes within the kerogen also suggests an incompletely anoxic environment, since *n*-aldehydes are usually presumed to be the intermediate products in the evolution of *n*-alcohols to fatty acids (Goodwin and Mercer, 1983; Schulte and Shock, 1993). In fact, the suggestion of a partial anoxic environment of the Lucaogou Formation is consistent with the viewpoints expressed in prior studies (Zhang et al., 2017, 2018; Tao et al., 2017).

5.2. Formation and evolution of long-chain oxygen-bearing compounds

5.2.1. Oxygen-bearing compounds occluded in the kerogen

Some ketone and aldehyde moieties, via ether-bonding combined with the kerogen network, would contribute to the formation of alkanones (van de Meent et al., 1980; Sinninghe Damsté et al., 1993; Riboulleau et al., 2000; Zhang et al., 2016; Zhang and Volkman, 2017) and *n*-aldehydes (Grasset, 1997; Gobé, 1998) when the ether bonds are thermally cracked. However, multiple series of the *n*-alkan-2-ones, fatty acid methyl esters and *n*-aldehydes, detected in this work from the H_2O_2 oxidation treatment of the isolated kerogen should belong to the occluded components of kerogen, but not the products via the ether-bonds cracking nor the oxidation outcomes of the substituted moieties chemically bonded to the kerogen. This can be verified by the following points:

(1) In our previous work, a series of thermal pyrolysis experiments were performed on this kerogen under different temperatures of 280 °C, 380 °C, 420 °C, 480 °C and 560 °C for 72 h, respectively, the extracted pyrolysis residues were then subjected to the H_2O_2 treatment, but no such oxygen-bearing compounds reported above were determined

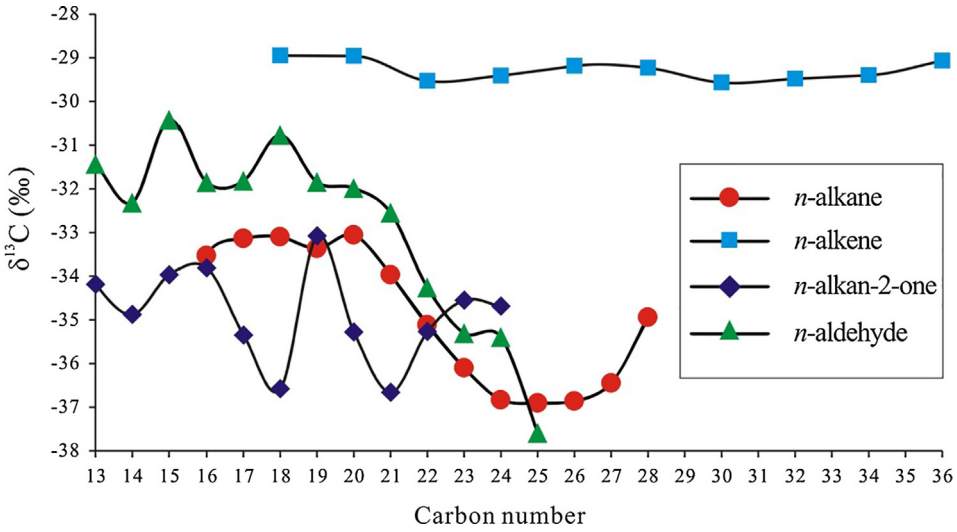

Fig. 8. $\delta^{13}C$ composition of individual compounds from the *n*-hexane extracts of kerogen and the oxidative degradation products. Note: The *n*-alkanes and *n*-alkan-2-ones are from the *n*-hexane fraction. The *n*-alk-1-enes and *n*-aldehydes are from the oxidative degradation products.

(Cheng et al., 2016). Therefore, these oxygen-bearing compounds detected in the present study were not from the oxidation products of the substituted moieties chemically bonded to kerogen, and it seems that these compounds have been destroyed under pyrolysis conditions and thus not determined from the H_2O_2 oxidation treatment of the pyrolysis residues.

(2) For the *n*-alkan-ones, the ratios of *n*-alkan-(4–9)-ones/*n*-alkan-2-ones showed almost the same distributional features with increasing carbon numbers in the *n*-hexane fraction and the oxidation degradation products (Fig. 5), which further suggested that the *n*-ketones detected in the oxidation products belong to the occluded components in kerogen rather than the reaction products from the substituted moieties chemically bonded to kerogen.

(3) The inter-correlated $\delta^{13}C$ distribution features of the short-chain *n*-aldehydes (occluded) and the *n*-alk-2-ones (adsorbed), as well as of the long-chain *n*-aldehydes (occluded) and the *n*-alkanes (adsorbed) (Fig. 8) also suggested that the aldehydes were indigenous to the sample but not an artifact of the H_2O_2 oxidation treatment.

(4) These oxygen-bearing compounds were all determined in the solvent extracted fractions (adsorbed compounds) of the isolated kerogen with similar distribution features to those in the oxidation products (Figs. 4, 6, and 7; Table 7), which indicates that the adsorbed and occluded fractions both belonged to the free components present as non-covalently bonded molecules in the kerogen structure.

5.2.2. Origin of the occluded n-aldehydes

In Fig. 8, the inter-correlated $\delta^{13}C$ distribution features of the short-chain *n*-aldehydes and the *n*-alk-2-ones, as well as of the long-chain *n*-aldehydes and the *n*-alkanes, indicated that the *n*-aldehydes had a close evolutionary relationship to the *n*-alkan-2-ones or *n*-alkanes. However, the occluded *n*-aldehydes could not have originated from the adsorbed *n*-alkan-2-ones or *n*-alkanes, as their formation should be no later than those of the adsorbed *n*-alkan-2-ones or *n*-alkanes with respect to the kerogen adsorption/occlusion behavior.

The *n*-aldehydes has been identified in several plant waxes (Tulloch, 1976; Prasad and Gülz, 1990; Gülz et al., 1989, 1992), sediments (Prahl and Pinto, 1987; Wünsche et al., 1988; Hostettler et al., 1989; Stephanou, 1989; Rieley et al., 1991; Püttmann and Bracke, 1995; Gogou and Stephanou, 2004; Tu et al., 2017), oil shales (Cardoso and Chicarelli, 1983) and in environmental particulate matter (Wils et al., 1982). The similar distribution pattern between the *n*-aldehydes and the *n*-alcohols or *n*-alkanes has been considered as evidence that the *n*-aldehydes originated from the oxidation of *n*-alcohols (Püttmann and Bracke, 1995; Gelin et al., 1994; Hartgers et al., 1995) or *n*-alkanes (Cardoso and Chicarelli, 1983; Albaigés et al., 1984; Stephanou, 1989), although a different view was noted by Wünsche et al. (1988). The *n*-aldehydes may also originate from the cleavage of an ether group in geomacromolecules (Grasset, 1997; Gobé, 1998), or from the hydrolysis and oxidation of alkanes at high temperature, as has been demonstrated by some laboratory experiments (Schulte and Shock, 1993; Leif et al., 1992).

Even carbon-numbered *n*-aldehydes have often been found in sediments (Prahl and Pinto, 1987; Wünsche et al., 1988; Hostettler et al., 1989; Püttmann and Bracke, 1995; Gogou and Stephanou, 2004; Feng et al., 2013; Tu et al., 2017) and in the pyrolysis products of soil macromolecular lipids (Gobé et al., 2000). However, in the present study the *n*-aldehydes in the occluded components did not show odd or even carbon number predominance. It seems that they may have formed during the diagenetic stage of the sedimentary organic matter, via the oxidation of *n*-alcohols, accompanied by kerogen formation and then occluded inside the kerogen.

5.2.3. Origin of the n-alkan-2-ones

The *n*-alkan-2-ones were detected in the adsorbed fraction as the main oxygen-bearing components, whereas in the occluded fraction *n*-aldehydes were determined to be the most abundant oxygen-bearing compounds. The *n*-alkan-2-ones are found in sediments or peat (Lehtonen and Ketola, 1990, 1993; Xie et al., 2004; Nichols and Huang, 2007; Zheng et al., 2007; Ortiz et al., 2010), and they are also detected in low maturity oil shale (Song et al., 2004). Prior studies have shown that *n*-alkan-2-ones may originate from the following pathways: (i) directly from the biota (Arpino et al., 1970; Volkman et al., 1981; Qu et al., 1999a; Baas et al., 2000; Hernández et al., 2001; Nichols and Huang, 2007; Jansen and Nierop, 2009; Ortiz et al., 2011); (ii) thermal degradation of geomacromolecules at a low maturity stage (Gillaizeau et al., 1996; Guignard et al., 2005; Zhang et al., 2016; Zhang and Volkman, 2017); (iii) microbial oxidation of the corresponding *n*-alkanes (Cranwell et al., 1987; Amblès et al., 1993; Jaffé et al., 1993,

1996; van Bergen et al., 1998); (iv) hydrolysis and oxidation of *n*-alkanes under radiolytic (Jaraula et al., 2015) or hydrothermal alterations (Leif and Simoneit, 1995, 2000); and (v) microbially assisted β-oxidation and decarboxylation of fatty acids (Volkman et al., 1983; Chaffee et al., 1986; de Leeuw, 1986; Quénéa et al., 2004).

The *n*-alkan-2-ones originating from pathways (i) or (ii) usually display an odd carbon-numbered predominance (Arpino et al., 1970; Volkman et al., 1981; Gillaizeau et al., 1996; Guignard et al., 2005; Ortiz et al., 2011; Zhang et al., 2016; Zhang and Volkman, 2017), which is not consistent with the present results from the *n*-hexane fraction (Fig. 4a). Although the Lucaogou kerogen was affected by biodegradation, the above pathway (iii) involving microbial alteration of *n*-alkanes is not the main source of the *n*-alkan-2-ones, because no *n*-alk-3-ones were detected from the occluded fraction which should be detected in the biodegradation products (Tuo and Li, 2005). Regarding pathway (iv), the radiolytic alteration mechanism reported by Jaraula et al. (2015) may not be the source of *n*-alkan-2-ones detected in this present work, because a very low uranium content has been reported for the Lucaogou Formation mudstones (Tao et al., 2017; Zhang et al., 2017).

Hydrothermal alteration of *n*-alkanes by pathway (iv) may have contributed to the formation of *n*-alkan-2-ones, because active hydrothermal fluid movements occurred during the formation and evolution of the Lucaogou Formation source rocks (Liu et al., 2012; Li et al., 2013; Hackley et al., 2016). Pathway (v), microbially assisted β-oxidation and decarboxylation of fatty acids, cannot be excluded as the source of *n*-alkan-2-ones detected here as the associated fatty acids and fatty acid methyl esters were simultaneously determined. Since the *n*-aldehydes are presumed to be intermediate products during the evolution from *n*-alcohols to fatty acids (Goodwin and Mercer, 1983; Schulte and Shock, 1993), thus it seems that the origins of the series of oxygen-bearing compounds detected in this work are inter-correlated between the *n*-alkan-2-ones, *n*-aldehydes, fatty acid methyl esters, *n*-alcohols and *n*-alkanes.

The inter-correlated variation of the $\delta^{13}C$ values between *n*-aldehydes and *n*-alkan-2-ones in Fig. 8 implies that they were closely related. One possible explanation is that bacterially mediated methylation of the *n*-aldehydes can generate the one carbon more *n*-alkan-2-ones with the latter more depleted in ^{13}C, which is likely to occur as the severe biodegradation has been observed in the Lucaogou Formation (Wang et al., 2012, 2016).

In Fig. 4, besides the abundant *n*-alkan-2-ones, some *n*-alkan-(3–9)-ones were also detected both in the adsorbed and occluded (except *n*-alkan-3-ones) fractions. These *n*-ketones may have originated from similar pathways as the dominant *n*-alkan-2-ones discussed above but with a much lesser production. They may have mainly originated from the hydrolysis and oxidation of *n*-alkanes through hydrothermal activity, possibly in combination with microbially assisted oxidation and decarboxylation of fatty acids.

5.2.4. Origin of the isoprenoid alkan-2-ones and fatty acid methyl esters

Besides the series of *n*-ketones, 6,10,14-trimethylpentadecan-2-one has been determined in both the adsorbed and occluded fractions (Fig. 4). The detection of 6,10,14-trimethylpentadecan-2-one is common in sediments (Rontani and Volkman, 2003; Nassiry et al., 2009), and may be produced via the following pathways: (i) from free phytol by aerobic or anaerobic biodegradation; (ii) by photosensitized oxidation of some specific isoprenoid hydrocarbons or tocopherols; and (iii) by the hydrolysis of chlorophyll-*a* photoproducts or the alkaline hydrolysis of tocopherols. The last pathway may be the origin of this compound detected in this present work, as the hydrothermal fluids extensively occurred in the Lucaogou Formation rocks. The $\delta^{13}C$ value of the isomeric 6,10,14-trimethylpentadecan-2-one is more enriched than those of the *n*-alkan-2-ones, indicating different formation and/or evolution pathways.

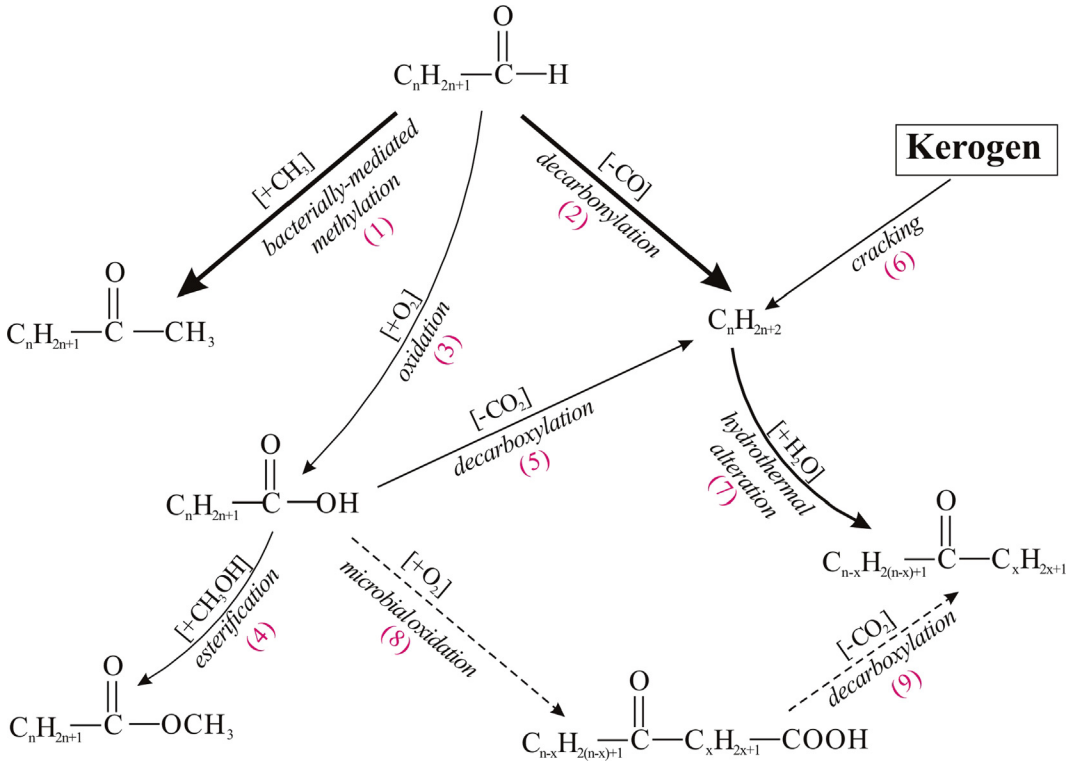

Fig. 9. Schematic evolution pathways of the oxygen-bearing compounds detected in this work. Note: The letters "n" and "x" represent carbon numbers.

Fatty acid methyl esters have been found in some organisms (Laseter and Weete, 1971; Matsuo et al., 1971; Hess et al., 1972; Robinson et al., 1987; Li et al., 2010) and sediments (Kennicutt and Jeffrey, 1981a,b; Qu et al., 1999b; Tuo et al., 2006; Li et al., 2008). A series of fatty acid methyl esters have been detected both in the adsorbed and occluded fractions (Fig. 6), so they may have originated from a secondary reaction by the methylation of fatty acids.

5.3. Mutually correlated evolution of the oxygen-bearing compounds

From the above discussion it seems that the sources and evolution of the *n*-aldehydes, *n*-alkan-2-ones (including some mid-chain ketones), fatty acid methyl esters and *n*-alkanes reported in this work were mutually correlated. The possible formation and evolution pathways of these compounds are illustrated in Fig. 9, which can be roughly classed into three stages. The first one was in a dysoxic to anoxic sedimentation stage, mainly comprising pathways (1) and (2), as well as the secondary reaction pathways (3), (4) and (5) in Fig. 9. The second stage was controlled by hydrothermal fluid movement, and mainly contained pathways (6) and (7). The third stage consisted of aerobic oxidation/biodegradation accompanied by crustal uplift, and mainly contained pathways (3) and (4), possibly as well as pathways (8) and (9) illustrated in Fig. 9.

During the kerogen formation stage, the *n*-aldehydes were not completely oxidized into fatty acids under a dysoxic sediment environment, so some *n*-aldehydes could be trapped inside the kerogen structures and then survived over subsequent geological evolution. While those *n*-aldehydes, weakly adsorbed to the kerogen or dispersed in the rocks, might be methylated into the one-more-carbon *n*-alkan-2-ones by bacterially assisted pathway (1). Some exposed *n*-aldehydes could be decarbonylated to form *n*-alkanes via pathway (2), or they could be oxidized into fatty acids via pathway (3) and then subsequently either esterified to generate fatty acid methyl esters via pathway (4) or decarboxylated to form *n*-alkanes via pathway (5) as illustrated in Fig. 9.

During the kerogen's diagenesis stage in the Lucaogou Formation, the hydrothermal fluid movements increased the environmental temperature, and under thermal stress some kerogen could be cracked to generate *n*-alkanes via pathway (6). Some *n*-alkanes could be transformed to the *n*-alkan-2-ones (including some mid-chain ketones) by hydrothermal alteration via pathway (7) (Leif and Simoneit, 1995, 2000). Crustal movement afterwards uplifted the Yuejinggou section of the Lucaogou Formation to the surface, and then the aerobic oxidation was enhanced, thus some remained *n*-aldehydes were oxidized into fatty acids via pathway (3), and subsequently further oxidized, under microbial assistance, into carbonyl fatty acids via pathway (8). As well, the oxidation products of the fatty acids could be decarboxylated to generate *n*-alkan-2-ones (including some mid-chain ketones) via pathway (9) as illustrated in Fig. 9.

6. Conclusions

Besides series of *n*-alkanes and *n*-alkenes, multiple series of oxygen-bearing compounds including *n*-ketones, *n*-aldehydes and fatty acid methyl esters have been detected in the adsorbed and occluded fractions of kerogen from the Lucaogou Formation of Santanghu Basin, NW China. The adsorbed fraction was dominated by *n*-alkan-2-ones whereas the occluded fraction was predominated by *n*-aldehydes. The *n*-aldehydes and the *n*-alkan-2-ones showed a similar carbon number distribution. The adsorbed fraction generally had a higher ratio of *n*-alkan-(4–9)-one/*n*-alkan-2-one compared to the occluded fraction. For the *n*-alk-1-enes, *n*-aldehydes, *n*-alkanes and *n*-alkan-2-ones with the same carbon number, the order of $\delta^{13}C$ values was basically *n*-alk-1-enes > *n*-aldehydes > *n*-alkanes > *n*-alkan-2-ones. In particular the C_{15} and C_{18} *n*-aldehydes were enriched in ^{13}C compared to their neighbors, which was accompanied by the corresponding C_{16} and C_{19} *n*-alkan-2-ones also enriched in ^{13}C compared to their neighboring carbon numbers.

Accompanying the kerogen's formation stage, some *n*-aldehydes could be occluded inside the kerogen structure and then survived. Some *n*-aldehydes dispersed outside the kerogen in the rocks may have experienced three main kinds of geochemical evolution: (1) gained a methyl group at the carbonyl carbon by methylation to generate one-more-carbon *n*-alkan-2-ones via bacterially assisted pathway; (2) the *n*-aldehydes and their corresponding fatty acids were decarbonylated to generate *n*-alkanes; (3) less likely, fatty acids derived from the *n*-aldehydes were further esterified to generate fatty acid methyl esters.

Crustal movement afterwards uplifted the Yuejinggou section of the Lucaogou Formation to the surface, so that aerobic oxidation was enhanced and any remaining *n*-aldehydes were oxidized to fatty acids, which could be subsequently further microbially oxidized into carbonyl fatty acids. The oxidation products of the fatty acids could be decarboxylated to generate *n*-alkan-2-ones, as well as some mid-chain ketones.

Acknowledgements

We are very grateful to John Volkman, Kliti Grice and the two anonymous reviewers for their careful reviews and valuable comments which significantly improved the quality of the manuscript. This work was financially supported by the National Natural Science Foundation of China (grant nos. 41502128 and 41472109) and the CAS XDB10010203.

Associate Editor—**Kliti Grice**

References

Albaigés, J., Algaba, J., Grimalt, J., 1984. Extractable and bound neutral lipids in some lacustrine sediments. Organic Geochemistry 6, 223–236.
Amblès, A., Jambu, P., Jacquesy, J.C., Parlanti, E., Secouet, B., 1993. Changes in the ketone portion of lipidic components during the decomposition of plant debris in a hydromorphic forest-podzol. Soil Science 156, 49–56.
Arpino, P., Albrecht, P., Ourisson, G., 1970. Series homologues aliphatics dans un sediment Eocène d'origen lacustre. Comptes Rendus Academie de Science, Series D 270, 1760–1763.
Baas, M., Pancost, R., van Geel, B., Sinninghe Damsté, J.S., 2000. A comparative study of lipids in Sphagnum species. Organic Geochemistry 31, 535–541.
Bao, J.P., 1997. 25-Norhopane series in the unbiodegraded oil and the source rocks. Chinese Science Bulletin 42, 1388–1391.
Behar, F., Pelet, R., Roucache, J., 1984. Geochemistry of asphaltenes. Organic Geochemistry 16, 587–595.
Blanc, P., Connan, J., 1992. Origin and occurrence of 25-norhopanes: a statistical study. Organic Geochemistry 18, 813–828.
Cardoso, J.N., Chicarelli, M.I., 1983. The organic geochemistry of the Paraiba Valley and Marau oil-shales. In: Bjorøy, M., Albrecht, P., Cornford, C., et al. (Eds.), Advances in Organic Geochemistry 1981. John Wiley, Chichester, pp. 828–833.
Cassani, F., Eglinton, G., 1986. Organic geochemistry of Venezuelan extra-heavy oils. 1. Pyrolysis of asphaltenes: a technique for the correlation and maturity evaluation of crude oils. Chemical Geology 56, 167–183.
Chaffee, A.L., Hoover, D.S., Johns, R.B., Schweighardt, F.K., 1986. Biological markers extractable from coal. In: Johns, R.B. (Ed.), Biological Markers in the Sedimentary Record. Elsevier, Amsterdam, pp. 311–345.
Cheng, B., Yang, C.P., Du, J.Y., Zhao, J., Liao, Z.W., 2014a. Determination of the series of even carbon numbered *n*-alk-(1)-enes trapped inside geomacromolecules. Marine and Petroleum Geology 51, 49–51.
Cheng, B., Hu, S.Z., Shen, C.B., Liao, Z.W., Liu, H., Du, J.Y., Tian, Y.K., 2014b. The geochemical characterization of adsorbed/occluded hydrocarbons inside solid bitumen in the Kuangshanliang area of northwestern Sichuan Basin and its significance. Petroleum Science and Technology 32, 2203–2211.
Cheng, B., Liao, Z.W., Wang, T.S., Liu, H., Tian, Y.K., Yang, S., 2015. Multiple charges to Sinian reservoirs in the middle Sichuan basin, SW China, insight from the adsorbed/occluded hydrocarbons in solid bitumens. Journal of Petroleum Science and Engineering 127, 359–366.

Cheng, B., Du, J.Y., Tian, Y.K., Liu, H., Liao, Z.W., 2016. Thermal evolution of adsorbed/occluded hydrocarbons inside kerogens and its significance as exemplified by one low–matured kerogen from Santanghu Basin, Northwest China. Energy & Fuels 30, 4529–4536.

Cheng, B., Zhao, J., Yang, C.P., Tian, Y.K., Liao, Z.W., 2017. Geochemical evolution of occluded hydrocarbons inside geomacromolecules: a review. Energy & Fuels 31 (9), 8823–8832.

Cranwell, P.A., Eglinton, G., Robinson, N., 1987. Lipids of aquatic organisms as potential contributors to lacustrine sediments – II. Organic Geochemistry 11, 513–527.

de Leeuw, J.W., 1986. Higher-molecular-weight markers. In: Johns, R.B. (Ed.), Biological Markers in the Sedimentary Record. Elsevier, Amsterdam, pp. 249–260.

Du, H.Y., Wang, T.G., Hu, J.L., Xu, G.F., 2004. 25-Norhopane in the source rock of Santanghu Basin and the function of microbe degradation. Petroleum Exploration & Development 31, 42–44 (in Chinese with English abstract).

Ekweozor, C.M., 1984. Tricyclic terpenoid derivatives from chemical degradation reactions of asphaltenes. Organic Geochemistry 6, 51–61.

Ekweozor, C.M., 1986. Characterization of the non-asphaltene products of mild chemical degradation of asphaltenes. Organic Geochemistry 10, 1053–1058.

Feng, X., Benitez-Nelson, B.C., Montluçon, D.B., Prahl, F.G., McNichol, A.P., Xu, L., Repeta, D.J., Eglinton, T.I., 2013. ^{14}C and ^{13}C characteristics of higher plant biomarkers in Washington margin surface sediments. Geochimica et Cosmochimica Acta 105, 14–30.

Gao, G., Li, H.M., Liang, H., 2010. Origin of Jurassic hydrocarbon and accumulation model in Santanghu Basin. Natural Gas Geoscience 21, 15–18 (in Chinese with English abstract).

Gelin, F., de Leeuw, J.W., Sinninghe Damsté, J.S., Derenne, S., Largeau, C., Metzger, P., 1994. Scope and limitations of flash pyrolysis-gas chromatography/mass spectrometry as revealed by the thermal behaviour of high-molecular-weight lipids derived from the green microalga *Botryococcus braunii*. Journal of Analytical and Applied Pyrolysis 28, 183–204.

George, S.C., Jardine, D.R., 1994. Ketones in a Proterozoic dolerite sill. Organic Geochemistry 21, 829–839.

Gillaizeau, B., Derenne, S., Largeau, C., Berkaloff, C., 1996. Source organisms and formation pathway of the kerogen of the Göynük Oil Shale (Oligocene, Turkey) as revealed by electron microscopy, spectroscopy and pyrolysis. Organic Geochemistry 24, 671–679.

Gobé, V., 1998. Matiére organique complexe du sol. Structure et rôle dans les processus d'humification du carbone xénobiotique. Ph.D. thesis. University of Poitiers, 224 pp.

Gobé, V., Lemée, L., Amblès, 2000. Structure elucidation of soil macromolecular lipids by preparative pyrolysis and thermochemolysis. Organic Geochemistry 31, 409–419.

Gogou, A., Stephanou, E., 2004. Marine organic geochemistry of the Eastern Mediterranean: 2. Polar biomarkers in Cretan Sea surficial sediments. Marine Chemistry 85, 1–25.

Goodwin, T.W., Mercer, E.I., 1983. Introduction to Plant Biochemistry, second ed. Pergamon Press, 677 pp.

Grasset, L., 1997. Etude de l'humine et des acides humiques des sols: Importance de la composante lipidique. Ph.D. thesis. University of Poitiers (France), 294 pp.

Grice, K., Schouten, S., Blokker, P., Derenne, S., Largeau, C., Nissenbaum, A., Sinninghe Damsté, J.S., 2003. Structural and isotopic analysis of kerogens in sediments rich in free sulfurised *Botryococcus braunii* biomarkers. Organic Geochemistry 34, 471–482.

Guignard, C., Lemée, L., Amblès, A., 2005. Lipid constituents of peat humic acids and humin. Distinction from directly extractable bitumen components using TMAH and TEAAc thermochemolysis. Organic Geochemistry 36, 287–297.

Gülz, P.G., Müller, E., Prasad, R.B.N., 1989. Organ-specific composition of epicuticular waxes of beech (*Fagus sylvatica* L.) leaves and seeds. Zeitschrift für Naturforschung C 44(9–10), 731–734.

Gülz, P.G., Müller, E., Hermann, T., 1992. Chemical composition and surface structures of epicuticular leaf waxes from *Castanea sativa* and *Aesculus hippocastanum*. Zeitschrift für Naturforschung C 47 (9–10), 661–666.

Hackley, P.C., Fishman, N., Wu, T., Baugher, G., 2016. Organic petrology and geochemistry of mudrocks from the lacustrine Lucaogou Formation, Santanghu Basin, northwest China: application to lake basin evolution. International Journal of Coal Geology 138, 20–34.

Hartgers, W.A., Sinninghe Damsté, J.S., de Leeuw, J.W., 1995. Curie-point pyrolysis of sodium salts of functionalized fatty acids. Journal of Analytical and Applied Pyrolysis 34, 191–217.

Hess, S.L., Weete, J.D., Gunasekaran, M., 1972. Changes in esters of fatty acids of *Rhizopus arrhizus* during germination and growth. Journal of Bacteriology 112 (1), 622–623.

Hernández, M.E., Mead, R., Peralba, M.C., Jaffé, R., 2001. Origin and transport of *n*-alkan-2-ones in a subtropical estuary: potential biomarkers for seagrass-derived organic matter. Organic Geochemistry 32, 21–32.

Hostettler, F.D., Rapp, J.B., Kvenvolden, K.A., Luoma, S.N., 1989. Organic markers as source discriminants and sediment transport indicators in south San Francisco Bay, California. Geochimica et Cosmochimica Acta 53, 1563–1576.

Jaffé, R., Cabrera, A., Hausmann, K., Carvajal-Chitty, H., 1993. On the origin and fate of *n*-alkane-2-ones in freshwater environments. In: Manning, D. (Ed.), Organic Geochemistry: Applications in Energy and the Natural Environment. Manchester University Press, Manchester, pp. 356–359.

Jaffé, R., Elisme, T., Cabrera, A.C., 1996. Organic geochemistry of seasonally flooded rain forest soils: molecular composition and early diagenesis of lipid components. Organic Geochemistry 25, 9–17.

Jansen, B., Nierop, K.G.J., 2009. Methyl ketones in high altitude Ecuadorian Andosols confirm excellent conservation of plant-specific *n*-alkane patterns. Organic Geochemistry 40, 61–69.

Jaraula, C.M.B., Schwark, L., Moreau, X., Pickel, W., Bagas, L., Grice, K., 2015. Radiolytic alteration of biopolymers in the Mulga Rock (Australia) uranium deposit. Applied Geochemistry 52, 97–108.

Jiang, Z.S., Fowler, M.G., Lewis, C.A., Philp, R.P., 1990. Polycyclic alkanes in a biodegraded oil from the Kelamayi oilfield, northwestern China. Organic Geochemistry 15, 35–46.

Jones, B., Manning, D.A.C., 1994. Comparison of geochemical indices used for the interpretation of palaeoredox conditions in ancient mudstones. Chemical Geology 111, 111–129.

Kennicutt, I.M.C., Jeffrey, L.M., 1981a. Chemical and GC–MS characterization of dissolved lipids. Martine Chemistry 10, 367–387.

Kennicutt, I.M.C., Jeffrey, L.M., 1981b. Chemical and GC–MS characterization of marine particulate lipids. Martine Chemistry 10, 389–407.

Khaddor, M., Ziyad, M., Amblès, A., 2008. Structural characterization of the kerogen from Youssoufia phosphate formation using mild potassium permanganate oxidation. Organic Geochemistry 39, 730–740.

Laseter, J.L., Weete, J.D., 1971. Fatty acid ethylesters of *Rhizopus arrhizus*. Science 172, 864–865.

Leif, R.N., Simoneit, B.R.T., Kvenvolden, K.A., 1992. Hydrous pyrolysis of *n*-$C_{32}H_{66}$ in the presence and absence of inorganic components. American Chemical Society Division of Fuel Chemistry Preprints 37 (4), 1748–1753.

Leif, R.N., Simoneit, B.R.T., 1995. Ketones in hydrothermal petroleums and sediment extracts from Guaymas Basin, Gulf of California. Organic Geochemistry 23, 889–904.

Leif, R.N., Simoneit, B.R.T., 2000. The role of alkenes produced during hydrous pyrolysis of a shale. Organic Geochemistry 31, 1189–1208.

Lehtonen, K., Ketola, M., 1990. Occurrence of long-chain acyclic methyl ketones in *Sphagnum* and *Carex* peats of various degrees of humification. Organic Geochemistry 15, 275–280.

Lehtonen, K., Ketola, M., 1993. Solvent-extractable lipids of *Sphagnum*, *Carex*, *Bryales*, and *Carex-Bryales* peats: content and compositional features vs. peat humification. Organic Geochemistry 15, 275–280.

Li, H., Liu, Y.Q., Liu, Y.L., Jiang, G.B., 2004. Analysis of the subsidence history of Tiaohu and Malang Sags of Santanghu Basin. Journal of Northwest University (Natural Science Edition) 34, 721–725 (in Chinese with English abstract).

Li, W., Liu, Y.Q., Dong, Y.P., Zhou, X.H., Liu, X.M., Li, H., Fan, T.T., Zhou, D.W., Xu, X.Y., Chen, J.L., 2013. The geochemical characteristics, geochronology and tectonic significance of the Carboniferous volcanic rocks of the Santanghu area in northeastern Xinjiang, China. Science China Earth Sciences 56, 1318–1333.

Li, Q.L., Wang, N.L., Wu, X.B., Pu, J.C., He, J.Q., Jiang, X., 2008. Composition and sources of biomarkers from surface sediment in Qiyi glacier, Qilian Mountains. Geochimica 37 (6), 533–541 (in Chinese with English abstract).

Li, W.M., Liang, H., 2001. The sedimentary environment of Lucaogou Formation in Upper Permian in Santanghu Basin. Xinjiang Petroleum 22, 497–498 (in Chinese with English abstract).

Li, Y.M., Wang, Y.L., He, D.X., Yang, H., Zhang, H., Wang, Y.X., Wen, Q.B., 2010. The characteristics of biomarkers in pine needles with different growing periods. Journal of Chinese Mass Spectrometry Society 31 (5), 313–320 (in Chinese with English abstract).

Liao, Z.W., Geng, A.S., 2002. Characterization of nC_7-soluble fractions of the products from mild oxidation of asphaltenes. Organic Geochemistry 33, 1477–1486.

Liao, Z.W., Geng, A.S., Graciaa, A., Creux, P., Chrostowska, A., Zhang, Y.X., 2006a. Saturated hydrocarbons occluded inside asphaltene structures and their geochemical significance, as exemplified by two Venezuelan oils. Organic Geochemistry 37, 291–303.

Liao, Z.W., Graciaa, A., Geng, A.S., Chrostowska, A., Creux, P., 2006b. A new low-interference characterization method for hydrocarbons occluded inside asphaltene structures. Applied Geochemistry 2006 (21), 833–838.

Lin, Q., Wang, J.S., Fu, H.F., Lu, H.F., Bu, Q.T., 2015. Elemental sulfur in northern South China Sea sediments and its significance. Science China Earth Sciences 45, 1747–1756.

Liu, B., Bechtel, A., Sachsenhofer, R.F., Gross, D., Gratzer, R., 2017. Depositional environment of oil shale within the second member of Permian Lucaogou Formation in the Santanghu Basin, Northwest China. International Journal of Coal Geology 175, 10–25.

Liu, B., Lü, Y.F., Meng, Y.L., Li, X.N., Guo, X.B., Ma, Q., Zhao, W.C., 2015. Petrologic characteristics and genetic model of lacustrine lamellar fine-grained rock and its significance for shale oil exploration: a case study of Permian Lucaogou Formation in Malang sag, Santanghu Basin, NW China. Petroleum Exploration and Development 42, 656–666.

Liu, X.W., Zheng, J.J., Yang, X., Liu, Y.H., 2010. Paleozoic structural evolution of Santanghu Basin and its surrounding and prototype basin recovery. Natural Gas Geoscience 21, 947–954 (in Chinese with English abstract).

Liu, Y.Q., Jiao, X., Li, H., Yuan, M.S., Yang, W., Zhou, X.H., Liang, H., Zhou, D.W., Zheng, C.Y., Sun, Q., Wang, S.S., 2012. Primary dolostone formation related to mantle-originated exhalative hydrothermal activities, Permian Yuejingou section, Santanghu area, Xinjiang, NW China. Science China Earth Sciences 55, 183–192.

Lockhart, R.S., Meredith, W., Love, G.D., Snape, C.E., 2008. Release of bound aliphatic biomarkers via hydropyrolysis from type II kerogen at high maturities. Organic Geochemistry 39 (8), 1119–1124.

Love, G.D., Snape, C.E., Fallick, A.E., 1998. Differences in the mode of incorporation and biogenicity of the principal aliphatic constituents of a Type I oil shale. Organic Geochemistry 28, 797–811.
Ma, J., Huang, Z.L., Li, H.M., Wu, H.Z., 2012. Matching relationship between faults and source rock and vertical migration characteristics of the oil in the Malang sag. Acta Sedimentologica Sinica 30, 1140–1148 (in Chinese with English abstract).
Ma, J., Huang, Z.L., Liang, S.J., Liu, Z.Z., Liang, H., 2016. Geochemical and tight reservoir characteristics of sedimentary organic-matter-bearing tuff from the Permian Tiaohu Formation in the Santanghu Basin, Northwest China. Marine and Petroleum Geology 73, 405–418.
Matsuo, A., Nakayama, M., Hayashi, S., 1971. Fatty acid esters in the volatile oil from the liverwort, *Pellia fabbroniana*. Phytochemistry 10, 430–432.
Nassiry, M., Aubert, C., Mouzdahir, A., Rontani, J.F., 2009. Generation of isoprenoid compounds, notably prist-1-ene, via photo and autoxidative degradation of vitamin E. Organic Geochemistry 40, 38–50.
Nichols, J.E., Huang, Y., 2007. C_{23}–C_{31} *n*-alkan-2-ones are biomarkers for the genus *Sphagnum* in freshwater peatlands. Organic Geochemistry 38, 1972–1976.
Ortiz, J.E., Gallego, J.L.R., Torres, T., Díaz-Bautista, A., Sierra, C., 2010. Palaeoenvironmental reconstruction of Northern Spain during the last 8000 cal yr BP based on the biomarker content of the Roñanzas peat Bog (Asturias). Organic Geochemistry 41, 454–466.
Ortiz, J.E., Diaz-Bautista, A., Jose Aldasoro, J., Torres, T., Gallego, J.L.R., Moreno, L., Estebanez, B., 2011. *n*-Alkan-2-ones in peat-forming plants from the Roñanzas ombrotrophic bog (Asturias, northern Spain). Organic Geochemistry 42, 586–592.
Peters, K.E., Walters, C.C., Moldowan, J.M., 2005. The Biomarker Guide, Volume 2: Biomarker and Isotopes in Petroleum Exploration and Earth History. Cambridge University Press, Cambridge.
Püttmann, W., Bracke, R., 1995. Extractable organic compounds in the clay mineral sealing of a waste disposal site. Organic Geochemistry 23, 43–54.
Prahl, F.G., Pinto, L.A., 1987. A geochemical study of long-chain *n*-aldehydes in Washington coastal sediments. Geochimica et Cosmochimica Acta 51, 1573–1582.
Prasad, R.B.N., Gülz, P.-G., 1990. Epicuticular waxes from leaves of maple (*Acer pseudoplatanus* L.). Zeitschrift Für Naturforschung C 45, 599–601.
Qu, W.C., Dickman, M., Wang, S.M., Wu, R.J.W., Zhang, P.Z., Chen, J.F., 1999a. Evidence for an aquatic origin of ketones found in Taihu Lake sediments. Hydrobiologia 397, 149–154.
Qu, W.C., Wang, S.M., Zhang, P.Z., Chen, J.F., Wu, R.J., 1999b. Identification and significance of long chain fatty acid methyl ester in the surface sediment of Taihu Lake. Journal of Lake Sciences 11 (3), 245–250 (in Chinese with English abstract).
Quénéa, K., Derenne, S., Largeau, C., Rumpel, C., Mariotti, A., 2004. Variation in lipid relative abundance and composition among different particle size fractions of a forest soil. Organic Geochemistry 35, 1355–1370.
Riboulleau, A., Derenne, S., Sarret, G., Largeau, C., Baudin, F., Connan, J., 2000. Pyrolytic and spectroscopic study of sulphur-rich kerogen from the "Kashpir oil shales" (Upper Jurassic; Russian Platform). Organic Geochemistry 31, 1641–1661.
Rieley, G., Collier, R.J., Jones, D.M., Eglinton, G., 1991. The biogeochemistry of Ellesmere Lake, U.K. – I: source correlation of leaf wax inputs to the sedimentary lipid record. Organic Geochemistry 17, 901–912.
Robinson, N., Cranwell, P.A., Eglinton, G., Jaworski, G.H.M., 1987. Lipids of four species of freshwater dinoflagellates. Phytochemistry 26, 411–421.
Rontani, J.F., Volkman, J.K., 2003. Phytol degradation products as biogeochemical tracers in aquatic environments. Organic Geochemistry 34, 1–35.
Russell, C.A., Snape, C.E., Meredith, W., Love, G.D., Clarke, E., Moffatt, B., 2004. The potential of bound biomarker profiles released via catalytic hydropyrolysis to reconstruct basin charging history for oils. Organic Geochemistry 35, 1441–1459.
Schulte, M.D., Shock, E.L., 1993. Aldehydes in hydrothermal solution: standard partial molal thermodynamic properties and relative stabilities at high temperatures and pressures. Geochimica et Cosmochimica Acta 57, 3835–3846.
Sinninghe Damsté, J.S., de las Heras, F.X.C., van Bergen, P.F., de Leeuw, J.W., 1993. Characterization of Tertiary Catalan lacustrine oil shales: discovery of extremely organic sulphur-rich Type I kerogens. Geochimica et Cosmochimica Acta 57, 389–415.
Snowdon, L.R., Volkman, J.K., Zhang, Z.Z., Tao, G.L., Liu, P., 2016. The organic geochemistry of asphaltenes and occluded biomarkers. Organic Geochemistry 91, 3–15.
Song, G.J., Hui, R.Y., Ding, A.N., Lu, S.F., 2004. Geochemical characteristics of neutral bearing-oxygen compounds in source rocks of biogas, Binbei area, Songliao Basin. Natural Gas Geoscience 15, 360–366 (in Chinese with English abstract).
Steiner, M., Wallis, E., Erdtmann, B.D., Zhao, Y.L., Yang, R.D., 2001. Submarine-hydrothermal exhalative ore layers in black shales from South China and associated fossils-insights into a Lower Cambrian facies and bio-evolution. Palaeogeography, Palaeoclimatology, Palaeoecology 169, 165–191.
Stephanou, E., 1989. Long-chain *n*-aldehydes. Naturwissenschaften 76, 464–467.
Tao, S., Xu, Y.B., Tang, D.Z., Xu, H., Li, S., Chen, S.D., Liu, W.B., Cui, Y., Gou, M.F., 2017. Geochemistry of the Shitoumei oil shale in the Santanghu Basin, Northwest China: implications for paleoclimate conditions, weathering, provenance and tectonic setting. International Journal of Coal Geology 184, 42–56.
Tissot, B.P., Welte, D.H., 1984. Petroleum Formation and Occurrence. Springer-Verlag, New York.
Tu, T.T.N., Egasse, C., Anquetil, C., Zanetti, F., Zeller, B., Huon, S., Derenne, S., 2017. Leaf lipid degradation in soils and surface sediments: a litterbag experiment. Organic Geochemistry 104, 35–41.
Tulloch, A.P., 1976. Chemistry of waxes of higher plants. In: Kolattukudy, P.E. (Ed.), Chemistry and Biochemistry of Natural Waxes. Elsevier, Amsterdam, pp. 235–287.
Tuo, J.C., Zhang, M.F., Wang, X.B., 2006. The content and significance of fatty acid methyl esters in Dongsheng sedimentary Uranium ore deposits, Ordos basin, China. Acta Sedimentologica Sinica 24 (3), 432–439 (in Chinese with English abstract).
Tuo, J.C., Li, Q., 2005. Occurrence and distribution of long-chain acyclic ketones in immature coals. Applied Geochemistry 20, 533–568.
van Bergen, P.F., Nott, C.J., Bull, I.D., Poulton, P.R., Evershed, R.P., 1998. Organic geochemical studies of soils from the Rothamsted Classical Experiments – IV. Preliminary results from a study of the effect of soil pH on organic matter decay. Organic Geochemistry 29, 1779–1795.
van de Meent, D., Brown, S.C., Philp, R.P., Simoneit, B.R.T., 1980. Pyrolysis-high resolution gas chromatography and pyrolysis gas chromatography-mass spectrometry of kerogens and kerogen precursors. Geochimica et Cosmochimica Acta 44, 999–1013.
Vandenbroucke, M., Largeau, C., 2007. Kerogen origin, evolution and structure. Organic Geochemistry 38, 719–833.
Volkman, J.K., Smith, D.J., Eglinton, G., Forsberg, T.E.V., Corner, E.D.S., 1981. Sterol and fatty acid composition of four marine Haptophycean algae. Journal of the Marine Biological Association of the UK 61, 509–527.
Volkman, J.K., Farrington, J.W., Gagosian, R., Wakeham, S.G., 1983. Lipid composition of coastal sediments from the Peru upwelling region. In: Bjorøy, M., Albrecht, P., Cornford, C., et al. (Eds.), Advances in Organic Geochemistry 1981. John Wiley and Sons, New York, pp. 228–240.
Wang, Z.D., Tao, M.X., Liang, M.L., He, W.G., Li, Z.P., Xu, Y.C., 2012. Characteristics of organic geochemistry of Lucaogou Formation source rock, Upper Permian, Santanghu Basin. Acta Sedimentologica Sinica 30, 975–982 (in Chinese with English abstract).
Wang, Z.D., Liang, M.L., Qian, Y., Wang, Z.Y., Li, X.B., Li, Z.P., 2016. The oxygen-bearing geolipids in the Lucaogou shale of Upper Permian, Santanghu Basin, China. Organic Geochemistry 102, 59–66.
Wignall, P.B., Twitchett, R.J., 1996. Oceanic anoxia and the end Permian mass extinction. Science 272, 1155–1158.
Wils, E.R.S., Hulst, A.G., den Hartog, J.C., 1982. The occurrence of plant wax constituents in airborne particulate matter in an urbanized area. Chemosphere 11, 1087–1096.
Wu, L.L., Geng, A., 2016. Differences in the thermal evolution of hopanes and steranes in free and bound fractions. Organic Geochemistry 101, 38–48.
Wu, X.Z., Lang, F.J., Li, B.H., Qi, X.F., Liu, D.G., 2011. Structure evolution and petroleum accumulation of Santanghu Basin. Chinese Journal of Geology 46, 808–825 (in Chinese with English abstract).
Wünsche, L., Mendoza, Y.A., Gülaçar, F.O., 1988. Lipid geochemistry of a post-glacial lacustrine sediment. Organic Geochemistry 13, 1131–1143.
Xie, S., Nott, C.J., Avsejs, L.A., Maddy, D., Chambers, F.M., Evershed, R.P., 2004. Molecular and isotopic stratigraphy in an ombotrophic mire for paleoclimate reconstruction. Geochimica et Cosmochimica Acta 68, 2849–2862.
Xu, X.W., Jiang, N., Li, X.H., Qu, X., Yang, Y.H., Mao, Q., Wu, Q., Zhang, Y., Dong, L.H., 2013. Tectonic evolution of the East Junggar terrane: evidence from the Taheir tectonic window, Xinjiang, China. Gondwana Research 24, 578–600.
Yin, F.J., Liu, H.F., Hua, H., 2002. Late Permian sporopollen assemblage from Lucaogou Formation in Santanghu Basin. Oil & Gas Geology 23, 392–397 (in Chinese with English abstract).
Zhang, G.W., Tao, S., Tang, D.Z., Xu, Y.B., Cui, Y., Wang, Q., 2017. Geochemical characteristics of trace elements and Rare earth elements in Permian Lucaogou oil shale, Santanghu Basin. Journal of China Coal Society 42, 2081–2089 (in Chinese with English abstract).
Zhang, S.H., Liu, C.Y., Liang, H., Wang, J.Q., Bai, J.K., Yang, M.H., Liu, G.H., Huang, H.X., Guan, Y.Z., 2018. Paleoenvironmental conditions, organic matter accumulation, and unconventional hydrocarbon potential for the Permian Lucaogou Formation organic-rich rocks in Santanghu Basin, NW China. International Journal of Coal Geology 185, 44–60.
Zhang, Z.R., Volkman, J.K., Xie, X., Snowdon, L.R., 2016. Stepwise pyrolysis of the kerogen from the Huadian oil shale, NE China: algaenan-derived hydrocarbons and mid-chain ketones. Organic Geochemistry 91, 89–99.
Zhang, Z.R., Volkman, J.K., 2017. Algaenan structure in the microalga *Nannochloropsis oculata* characterized from stepwise pyrolysis. Organic Geochemistry 104, 1–7.
Zhao, J., Liao, Z.W., Zhang, L.H., Creux, P., Yang, C.P., Chrostowska, A., Zhang, H.Z., Graciaa, A., 2010. Comparative studies on compounds occluded inside asphaltenes hierarchically released by increasing amounts of H_2O_2/CH_3COOH. Applied Geochemistry 25, 1330–1338.
Zhao, J., Liao, Z.W., Chrostowska, A., Liu, Q., Zhang, L.Y., Graciaa, A., Creux, P., 2012. Experimental studies on the adsorption/occlusion phenomena inside the macromolecular structures of asphaltenes. Energy & Fuels 26, 1746–1755.
Zhao, Z.H., Guo, Z.J., Zhang, C., Lu, H.M., 2003. Tectonic evolution of the Santanghu Basin, East Xinjiang and its implication for the hydrocarbon accumulation. Acta Scientiarum Naturalium Universitatis Pekinensis 39, 219–228 (in Chinese with English abstract).
Zheng, Y., Zhou, W., Meyers, P.A., Xie, S., 2007. Lipid biomarkers in the Zoigê-Hongyuan peat deposit: indicators of Holocene climate changes in West China. Organic Geochemistry 38, 1927–1940.

View publication stats